

An effective operational matrix method based on barycentric cardinal functions to study nonlinear MHD nanofluid flow and heat transfer

S. Torkaman ^a, G.B. Loghmani ^a, M. Heydari ^a, M.M. Rashidi ^b

^aDepartment of Mathematics, Yazd University, Yazd, Iran

^bShanghai Automotive Wind Tunnel Center, Tongji University, No. 4800, Cao'an Road, Shanghai 201804, China

ABSTRACT: A two-dimensional incompressible viscous MHD nanofluid flow over a flat sheet with considering thermal radiation and buoyancy effects is investigated. An effective operational matrix-based method is used for the numerical simulation. At first, based on the barycentric rational cardinal functions, the operational matrices of integration and product are provided. Then, by employing the obtained operational matrices, the governing differential equations in differential form are reduced to a system of nonlinear algebraic equations. The effect of different physical parameters such as the magnetic parameter Mn , the buoyancy parameter λ , the nanoparticle volume fraction ϕ and the radiation parameter N on the temperature distribution, velocity profile, Nusselt number and skin friction coefficient is demonstrated by graphs and tables. Also, some comparisons with the obtained results of the numerical method based on Maple's `dsolve` (type=numeric) command and other existing numerical solutions are provided to confirm the accuracy and efficiency of the proposed method.

Keywords: Buoyancy effect; Thermal radiation; Barycentric interpolation; Operational matrices of integration and product

1. INTRODUCTION

The study of fluid flow over a stretching surface with heat transfer due to its extensive applications in engineering and technology has special importance in fluid mechanics. Some typical examples of this type of boundary-layer flow are in the metal and polymer sheets production, cooling of electronic chips, glass-fiber production, crystal growing, blood vessels, aerodynamic extrusion of plastic sheets, etc. The boundary-layer flow on continuous solid surfaces was first investigated by Sakiadis in [1, 2]. Then, Crane [3] studied the boundary-layer flow and heat transfer on a linearly stretching sheet. Since then, different features of this type of boundary-layer flow and associated problems have been studied by many authors [4-11]. Nanofluids are a combination of a base fluid with nanoparticles and base fluid such as water normally has a low value of thermal conductivity. Therefore, heat transfer can be increased by adding nanoparticles whose thermal conductivity is higher than the base fluid. The steady two-dimensional boundary layer flow problem over stretching flat surface in nanofluids, was first investigated numerically by Khan and Pop [12]. The problem of natural convection nanofluid flow on a linearly stretching surface in the presence of magnetic field analytically studied by Hamad [13]. Rashidi et al. [14] investigated the problem of steady second-order slip nanofluid flow of an incompressible viscous water-based nanofluid over a stretching/shrinking sheet and reported analytical and numerical solutions. Rana and

Bhargava [15] studied the steady two-dimensional boundary layer flow of a nanofluid past a nonlinearly stretching flat surface. They applied the variational finite element method (FEM) to solve the system of nonlinear differential equations. Hayat et al. [16] employed the homotopy analysis method (HAM) to find the approximate solution of the steady boundary layer flow of an incompressible nanofluid over an exponentially stretching surface in a porous medium. Reddy et al. [17] studied the MHD boundary-layer flow along with heat and mass transfer of Williamson nanofluid over a stretching plate by using the spectral quasi-linearisation method (SQLM). The nanofluid flow on a curved surface with nonlinear stretching velocity is analyzed by Hayat et al. [18]. They applied the HAM to find the approximate solution of governing differential equations.

In recent years, several studies based on the Chebyshev cardinal functions [19- 24], Chebyshev polynomials [25-29], Bernstein polynomials [30- 33], radial basis function [34- 36] have been provided to solve nonlinear differential equations. The main purpose of this research is to provide an efficient direct method based on the barycentric rational cardinal functions and associated operational matrices of integral and product for solving the problem of MHD nanofluid flow and heat transfer over a vertical stretching surface. The barycentric form of rational interpolants were presented in 1986 by Schneider and Werner [37]. In 1998, Berrut [38] provided a linear barycentric rational interpolation with no real poles. Then, in 2007, Floater and Hormann [39], with the combination of $(n - d + 1)$ local polynomials of degree

* Corresponding Author: mm_rashidi@yahoo.com (M.M. Rashidi) and loghmani@yazd.ac.ir (G.B. Loghmani).

at most d , provided a family of rational interpolants with high approximation order on the arbitrary interval $[a, b]$. Recently, linear barycentric rational interpolants have been utilized to obtain the approximate solutions of ordinary and partial differential equations, Volterra and Fredholm integral equations and integro-differential equations [40- 47].

The framework of this paper is organized as follows: In Section 2, the problem of two-dimensional nanofluid flow and heat transfer over a stretching surface is described. The barycentric rational cardinal functions and the associated operational matrices are demonstrated in Sections 3 and 4, respectively. In Section 5, the operational matrix-based method for solving governing differential equations is described. In Section 6, the convergence analysis of presented method is studied. The obtained numerical results are reported in Section 7. Finally, the conclusion is expressed in the last Section.

2 FORMULATION OF THE PROBLEM

Figure 1 shows the steady laminar two-dimensional fluid flow and heat transfer of an incompressible viscous nanofluid passing through a vertical semi-infinite sheet with considering a uniform magnetic field of strength B_0 . The flow direction is upward and the lateral direction is y direction, as can be seen in the below figure.

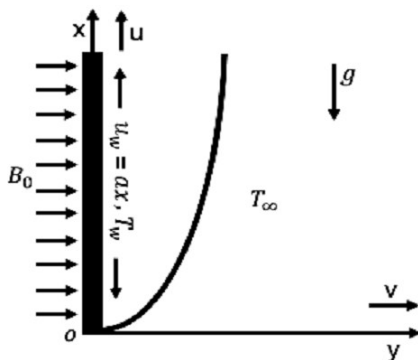


Fig. 1. Schematic of the MHD nanofluid flow and boundary layer.

The considered velocity distribution is $u_w(x) = ax$ and a represents the stretching factor. The temperature of the stretching sheet is T_w , and ambient temperature (temperature at infinity) is T_∞ . With a good approximation, one can neglect the slip between nanoparticles and base fluid, also two phase are in thermal equilibrium condition. By implementing the similarity transformations [50]

$$\eta = \sqrt{\frac{a}{v_f}} y, \quad u = axf'(\eta), \quad v = -\sqrt{av_f}f(\eta), \quad \theta(\eta) = \frac{T - T_\infty}{T_w - T_\infty}$$

The Navier-Stokes equations can be reduced to a set of nonlinear ODEs as follow:

$$f''' + (1 - \phi)^{2.5} \left[\left(1 - \phi + \frac{\rho_s}{\rho_f} \phi \right) (ff'' - f'^2) - Mn f' + \lambda \left(1 - \phi \frac{(\rho\beta)_s}{(\rho\beta)_f} \phi \right) \theta \right] = 0, \quad (1)$$

$$\theta'' + \frac{3N}{3N+4} \frac{k_f}{k_{nf}} Pr \left(1 - \phi + \frac{(\rho C_p)_s}{(\rho C_p)_f} \phi \right) f \theta' = 0, \quad (2)$$

The corresponding boundary conditions are:

$$\eta = 0: f = 0, f' = 1, \theta = 1, \quad (3)$$

$$\eta \rightarrow +\infty: f' \rightarrow 0, \theta \rightarrow 0, \quad (4)$$

where ϕ is the solid volume fraction, σ is the electric conductivity, β is the thermal expansion, $Mn = \frac{\sigma B_0^2}{\rho_f a}$ is the magnetic parameter, $N = \frac{k_{nf} k_{nf}^*}{4\sigma T_\infty^3}$ is the radiation parameter, k_{nf}^* is the mean absorption coefficient of the nanofluid, $Pr = \frac{v_f}{\alpha_f}$ is the Prandtl parameter, $\lambda = \frac{g\beta_f(T_w - T_\infty)}{au}$ is the buoyancy parameter and g is the acceleration due to gravity. Here, subscripts nf, f and s stand for nanofluid, based fluid and nano-solid-particles, respectively. So, ρ is the nanofluid density, k is the thermal conductivity, μ is the effective dynamic viscosity, (ρC_p) is the heat capacitance and are computed as follows[51]:

$$\begin{cases} (\rho C_p)_{nf} = (1 - \phi)(\rho C_p)_f + \phi(\rho C_p)_s, \\ (\rho\beta)_{nf} = (1 - \phi)(\rho\beta)_f + \phi(\rho\beta)_s, \\ k_{nf} = \frac{k_s + 2k_f - 2\phi(k_f - k_s)}{k_f - k_s + 2\phi(k_f - k_s)}, \\ \rho_{nf} = (1 - \phi)\rho_f + \phi\rho_s. \end{cases}$$

Also, the skin friction coefficient C_f and the reduced Nusselt number Nu are defined as:

$$C_f = -\frac{1}{(1 - \phi)^{2.5}} Re_x^{-\frac{1}{2}} f''(0),$$

$$Nu = -Re_x^{\frac{1}{2}} \left(\frac{3N+4}{3N} \right) \theta'(0),$$

where $\mu_{nf} = \frac{\mu_f}{(1 - \phi)^{2.5}}$, σ^* is the Stefan-Boltzmann constant [52] and $Re_x = \frac{xu_w}{v_f}$ denotes the local Reynolds number.

3 BARYCENTRIC RATIONAL CARDINAL FUNCTIONS

Suppose that $f: [a, b] \rightarrow \mathbb{R}, n \in \mathbb{N}$, $\Delta = \{a = \eta_0 < \eta_1 < \dots < \eta_n = b\}$ is a set of distinct points and $f_j = f(\eta_j)$ for $j = 0, 1, \dots, n$ are the given data.

Definition 3.1 For a given set of interpolation nodes such as Δ , the cardinal functions (cardinal basis) $\psi_j(\eta)$ are defined as [20, 48]:

$$\psi_j(\eta_i) = \delta_{ji}, \quad i, j = 0, 1, \dots, n, \quad (5)$$

where δ_{ji} is the Kronecker delta function.

Here, consider a set of cardinal functions based on the linear barycentric rational interpolation. A linear barycentric rational interpolant can be expressed as:

$$r_n(\eta) = \frac{\sum_{j=0}^n \frac{w_j}{\eta - \eta_j} f_j}{\sum_{i=0}^n \frac{w_i}{\eta - \eta_i}}, \quad (6)$$

where $\{w_j\}_{j=0}^n$ are arbitrary nonzero set of weights. Floater and Hormann [39] proposed a family of rational interpolants based on the barycentric weights w_j as follows:

$$w_j = (-1)^j \sum_{i=\max(j-d, 0)}^{\min(j, n-d)} \left(\prod_{k=i, k \neq j}^{i+d} \frac{1}{|\eta_j - \eta_k|} \right), \quad j = 0, 1, \dots, n. \quad (7)$$

The barycentric formula with the weights defined in (7) can be rewritten as:

$$r_n(\eta) = \frac{\sum_{i=0}^{n-d} \lambda_i(\eta) p_i(\eta)}{\sum_{i=0}^{n-d} \lambda_i(\eta)}, \quad \lambda_i(\eta) = \frac{(-1)^i}{(\eta - \eta_i) \dots (\eta - \eta_{i+d})}, \quad i = 0, 1, \dots, n-d, \quad (8)$$

where $0 \leq d \leq n$ is an integer parameter and $p_i(\eta)$ is the polynomial of degree at most d and interpolates $f(\eta)$ at local nodes $\eta_i, \dots, \eta_{i+d}$.

Now, using the interpolation formula (6), the barycentric rational cardinal functions $\psi_j(\eta)$, $j = 0, 1, \dots, n$ can be defined as follows:

$$\psi_j(\eta) = \frac{w_j}{\vartheta(\eta)(\eta - \eta_j)}, \quad j = 0, 1, \dots, n, \quad (9)$$

where

$$\vartheta(\eta) = \sum_{i=0}^n \frac{w_i}{\eta - \eta_i}$$

and $\{w_j\}_{j=0}^n$ are arbitrary nonzero numbers. From Definition 3.1, any function f on the interval $[a, b]$ may be approximated by cardinal functions (9) as:

$$f(\eta) \approx \sum_{j=0}^n f(\eta_j) \psi_j(\eta) = F^T \Psi(\eta), \quad (10)$$

where

$$F = [f(\eta_0), f(\eta_1), \dots, f(\eta_n)]^T, \quad \Psi(\eta) = [\psi_0(\eta), \psi_1(\eta), \dots, \psi_n(\eta)]^T.$$

Remark 3.2 Based on the Kronecker property (5), one can get

$$\Psi(\eta_j) = e_j, \quad j = 0, 1, \dots, n,$$

where e_j is the j -th column of unit matrix of order $n + 1$.

Theorem 3.3 [39] Suppose that $f \in C^{d+2}[a, b]$. Then

$$\|f - r_n\|_{\infty} \leq \begin{cases} h(1 + \beta)(b - a) \frac{\|f''\|_{\infty}}{2}, & d = 0, n \text{ odd}, \\ h(1 + \beta) \left((b - a) \frac{\|f''\|_{\infty}}{2} + \|f'\|_{\infty} \right), & d = 0, n \text{ even}, \\ h^{d+1}(b - a) \frac{\|f^{(d+2)}\|_{\infty}}{d + 2}, & d \geq 1, (n - d) \text{ odd}, \\ h^{d+1} \left((b - a) \frac{\|f^{(d+2)}\|_{\infty}}{d + 2} + \frac{\|f^{(d+1)}\|_{\infty}}{d + 1} \right), & d \geq 1, (n - d) \text{ even}, \end{cases}$$

where

$$h = \max_{0 \leq i \leq n-1} (\eta_{i+1} - \eta_i), \quad \beta = \max_{1 \leq i \leq n-2} \min \left(\frac{\eta_{i+1} - \eta_i}{\eta_i - \eta_{i-1}}, \frac{\eta_{i+1} - \eta_i}{\eta_{i+2} - \eta_{i+1}} \right).$$

4 OPERATIONAL MATRICES OF BARYCENTRIC RATIONAL CARDINAL FUNCTIONS

In this section, the operational matrices of integration and product based on the cardinal functions (9) will be derived. For this purpose, consider $\Psi(\eta)$ is a $(n + 1) \times 1$ vector as follows:

$$\Psi(\eta) = [\psi_0(\eta), \psi_1(\eta), \dots, \psi_n(\eta)]^T, \quad (11)$$

where $\{\psi_j(\eta)\}_{j=0}^n$ are the cardinal functions defined in (9).

Lemma 4.1 Let $\Psi(\eta)$ be the vector defined in (11), then

$$\int_a^\eta \Psi(s) ds \approx \mathbf{P} \Psi(\eta),$$

where $\mathbf{P} = (p_{ij})$ is the $(n + 1) \times (n + 1)$ operational matrix of integration and is defined as follows:

$$p_{ij} = \int_a^{\eta_j} \psi_i(\eta) d\eta, \quad i, j = 0, 1, \dots, n. \quad (12)$$

Proof. Using (10), any functions $\int_a^\eta \psi_i(s) ds$, $i = 0, 1, \dots, n$ can be estimated as

$$\int_a^\eta \psi_i(s) ds \approx \sum_{j=0}^n p_{ij} \psi_j(\eta), \quad i = 0, 1, \dots, n$$

where

$$p_{ij} = \int_a^{\eta_j} \psi_i(\eta) d\eta, \quad i, j = 0, 1, \dots, n.$$

So,

$$\int_a^{\eta} \Psi(s) ds = \left[\int_a^{\eta} \psi_0(s) ds, \int_a^{\eta} \psi_1(s) ds, \dots, \int_a^{\eta} \psi_n(s) ds \right]^T \\ \simeq \left[\sum_{j=0}^n p_{0j} \psi_j(\eta), \sum_{j=0}^n p_{1j} \psi_j(\eta), \dots, \sum_{j=0}^n p_{nj} \psi_j(\eta) \right]^T = \mathbf{P}\Psi(\eta). \quad \blacksquare$$

Remark 4.2 The entries of the operational matrix \mathbf{P} can be approximated by using the Legendre-Gauss-Lobatto quadrature rule as follows:

$$p_{ij} \simeq \frac{\eta_j - a}{2} \sum_{k=0}^M \tilde{\omega}_k \psi_i \left(\frac{\eta_j - a}{2} \tilde{\eta}_k + \frac{\eta_j + a}{2} \right), \quad i, j = 0, 1, \dots, n,$$

where $L_M(\eta)$ is the Legendre polynomial of order M on $[-1, 1]$, $\{\tilde{\eta}_k\}_{k=0}^M$ are the zeros of $(1 - \eta^2)L_M'(\eta)$ and

$$\tilde{\omega}_k = \frac{2}{M(M+1)} \frac{1}{(L_M(\eta_k))^2}, \quad k = 0, 1, \dots, M,$$

are the Legendre-Gauss-Lobatto weights [49]. Also, from (12), the following equation can be obtained:

$$p_{i0} = \int_a^{\eta_0} \psi_i(\eta) d\eta = 0, \quad i = 0, 1, \dots, n.$$

Remark 4.3 Let m and k be arbitrary integers, $m \geq k$ and

$$f^{(m)}(\eta) \simeq F^T \Psi(\eta), \quad (13)$$

where $F = [f^{(m)}(\eta_0), f^{(m)}(\eta_1), \dots, f^{(m)}(\eta_n)]^T$ and $\Psi(\eta)$ is the vector function described in (11). By integrating both sides of (13) from a to η , the below approximation can be derived:

$$f^{(m-1)}(\eta) \simeq f^{(m-1)}(a) + \int_a^{\eta} F^T \Psi(s) ds \simeq f^{(m-1)}(a) + F^T \mathbf{P}\Psi(\eta), \\ f^{(m-2)}(\eta) \simeq f^{(m-2)}(a) + f^{(m-1)}(a)(\eta - a) + \int_a^{\eta} F^T \mathbf{P}\Psi(s) ds \\ \simeq f^{(m-2)}(a) + f^{(m-1)}(a)(\eta - a) + F^T \mathbf{P}^2 \Psi(\eta).$$

By following the above process, it is observed that

$$f^{(m-k)}(\eta) \simeq v_{f,k}(\eta) + F^T \mathbf{P}^k \Psi(\eta), \quad (14)$$

where

$$v_{f,k}(\eta) = \sum_{j=1}^k \frac{f^{(m-j)}(a)}{(k-j)!} (\eta - a)^{k-j},$$

is a polynomial of order $k - 1$. Also, $v_{f,k}(\eta)$ can be approximated as follows:

$$v_{f,k}(\eta) \simeq \Lambda_{f,k}^T \Psi(\eta), \quad (15)$$

where

$$\Lambda_{f,k} = [v_{f,k}(\eta_0), v_{f,k}(\eta_1), \dots, v_{f,k}(\eta_n)]^T.$$

Finally, by substituting (15) in (14), we get

$$f^{(m-k)}(\eta) \simeq \underbrace{(\Lambda_{f,k}^T + F^T \mathbf{P}^k)}_{\tilde{F}_{m-k}} \Psi(\eta) = \tilde{F}_{m-k} \Psi(\eta), \quad k = 1, 2, \dots, m.$$

Lemma 4.4 Let $F = [f_0, f_1, \dots, f_n]^T$ be a column vector and $\Psi(\eta)$ be the vector function defined in (11), then

$$\Psi(\eta) \Psi^T(\eta) F \simeq \tilde{F} \Psi(\eta),$$

where \tilde{F} is a $(n + 1) \times (n + 1)$ product operational matrix and is defined as follows:

$$\tilde{F} = \text{diag}[f_0, f_1, \dots, f_n].$$

Proof. It is clear that $\Psi(\eta) \Psi^T(\eta)$ is a $(n + 1) \times (n + 1)$ matrix as

$$\Psi(\eta) \Psi^T(\eta) = \begin{bmatrix} \psi_0(\eta)\psi_0(\eta) & \psi_0(\eta)\psi_1(\eta) & \dots & \psi_0(\eta)\psi_n(\eta) \\ \psi_1(\eta)\psi_0(\eta) & \psi_1(\eta)\psi_1(\eta) & \dots & \psi_1(\eta)\psi_n(\eta) \\ \vdots & \vdots & \ddots & \vdots \\ \psi_n(\eta)\psi_0(\eta) & \psi_n(\eta)\psi_1(\eta) & \dots & \psi_n(\eta)\psi_n(\eta) \end{bmatrix}. \quad (16)$$

Using (10), any functions $\psi_i(\eta)\psi_j(\eta), i, j = 0, 1, \dots, n$ can be approximated as

$$\psi_i(\eta)\psi_j(\eta) \simeq \sum_{k=0}^n \psi_i(\eta_k)\psi_j(\eta_k)\psi_k(\eta), \quad i, j = 0, 1, \dots, n. \quad (17)$$

According to Kronecker property (5), we obtain

$$\psi_i(\eta_k)\psi_j(\eta_k) = \delta_{ik}\delta_{jk}.$$

Substituting (17) in (16) yields

$$\Psi(\eta) \Psi^T(\eta) \simeq \text{diag}[\psi_0(\eta), \psi_1(\eta), \dots, \psi_n(\eta)].$$

Now, by multiplying the vector F , the desired result is obtained. \blacksquare

5 DESCRIPTION OF THE COMPUTATIONAL TECHNIQUE

This section presents an effective operational matrix-based method for solving nonlinear differential equations (1) and (2) with the corresponding boundary conditions.

First, we replace the asymptotic boundary conditions (4) with the following conditions

$$\eta = L: f' = 0, \theta = 0, \tag{18}$$

where $L \in \mathbb{R}^+$ should be chosen sufficiently large. Then, by using the cardinal functions (9), $f'''(\eta)$ and $\theta''(\eta)$ can be approximated as follows:

$$f'''(\eta) \simeq F^T \Psi(\eta), \tag{19}$$

where

$$\begin{aligned} F &= [f_0, f_1, \dots, f_n]^T, \\ \Theta &= [\theta_0, \theta_1, \dots, \theta_n]^T, \end{aligned} \tag{20}$$

are unknown vectors and must be determined. By integrating from (19) and (20) over the interval $[0, \eta]$, the below approximations for velocity and temperature (and their derivatives) will be obtained:

$$\begin{aligned} f''(\eta) &\simeq f''(0) + F^T \mathbf{P} \Psi(\eta), \\ f'(\eta) &\simeq f'(0) + \eta f''(0) + F^T \mathbf{P}^2 \Psi(\eta), \\ f(\eta) &\simeq f(0) + \eta f'(0) + \frac{\eta^2}{2} f''(0) + F^T \mathbf{P}^3 \Psi(\eta), \end{aligned}$$

and

$$\begin{aligned} \theta'(\eta) &\simeq \theta'(0) + \Theta^T \mathbf{P} \Psi(\eta), \\ \theta(\eta) &\simeq \theta(0) + \eta \theta'(0) + \Theta^T \mathbf{P}^2 \Psi(\eta). \end{aligned}$$

By employing the initial condition (3), the below approximations can be obtained:

$$f''(\eta) \simeq f''(0) + F^T \mathbf{P} \Psi(\eta), \tag{21}$$

$$f'(\eta) \simeq 1 + \eta f''(0) + F^T \mathbf{P}^2 \Psi(\eta), \tag{22}$$

$$f(\eta) \simeq \eta + \frac{\eta^2}{2} f''(0) + F^T \mathbf{P}^3 \Psi(\eta), \tag{23}$$

and

$$\theta'(\eta) \simeq \theta'(0) + \Theta^T \mathbf{P} \Psi(\eta), \tag{24}$$

$$\theta(\eta) \simeq 1 + \eta \theta'(0) + \Theta^T \mathbf{P}^2 \Psi(\eta). \tag{25}$$

Using (22), (25) and boundary conditions (18), $f''(0)$ and $\theta'(0)$ can be computed as:

$$f''(0) \simeq \frac{-1 - F^T \mathbf{P}^2 \Psi(L)}{L},$$

$$\theta'(0) \simeq \frac{-1 - \Theta^T \mathbf{P}^2 \Psi(L)}{L}.$$

Now, using Remark 4.3, equations (21)-(25) can be simplified as follows:

$$f^{(3-k)}(\eta) \simeq (\Lambda_{f,k}^T + F^T \mathbf{P}^k) \Psi(\eta) = \hat{F}_{3-k} \Psi(\eta), \quad k = 1, 2, 3, \tag{26}$$

$$\theta^{(2-k)}(\eta) \simeq (\Lambda_{\theta,k}^T + \Theta^T \mathbf{P}^k) \Psi(\eta) = \hat{\Theta}_{2-k} \Psi(\eta), \quad k = 1, 2. \tag{27}$$

By applying (26), (27) and Lemma 4.4:

$$f(\eta) f''(\eta) \simeq \hat{F}_0 \underbrace{\Psi(\eta) \Psi^T(\eta) \hat{F}_2^T}_{\tilde{B}_1 \Psi(\eta)} \simeq \hat{F}_0 \tilde{B}_1 \Psi(\eta), \tag{28}$$

$$f'(\eta)^2 \simeq \hat{F}_1 \underbrace{\Psi(\eta) \Psi^T(\eta) \hat{F}_1^T}_{\tilde{B}_2 \Psi(\eta)} \simeq \hat{F}_1 \tilde{B}_2 \Psi(\eta), \tag{29}$$

$$f(\eta) \theta'(\eta) \simeq \hat{F}_0 \underbrace{\Psi(\eta) \Psi^T(\eta) \hat{\Theta}_1^T}_{\tilde{B}_3 \Psi(\eta)} \simeq \hat{F}_0 \tilde{B}_3 \Psi(\eta), \tag{30}$$

where $\tilde{B}_1, \tilde{B}_2, \tilde{B}_3$ are $(n+1) \times (n+1)$ diagonal matrices. By substituting (19), (20) and (26)-(30) in (1) and (2) and canceling $\Psi(\eta)$, one can obtain:

$$F^T + (1-\phi)^{2.5} \left\{ (1-\phi + \frac{\rho_s}{\rho_f} \phi) [\hat{F}_0 \tilde{B}_1 - \hat{F}_1 \tilde{B}_2] - Mn \hat{F}_1 + \lambda \left(1 - \phi + \frac{(\rho \beta)_s}{(\rho \beta)_f} \phi \right) \hat{\Theta}_0 \right\} = 0, \tag{31}$$

$$\Theta^T + \frac{3N}{3N+4} \frac{k_f}{k_{nf}} Pr \left(1 - \phi + \frac{(\rho C_p)_s}{(\rho C_p)_f} \phi \right) \hat{F}_0 \tilde{B}_3 = 0. \tag{32}$$

Finally, by solving the system of nonlinear algebraic equations (31) and (32), the unknown vectors F and Θ will be determined. Also, according to the above notations and Remark 3.2, the following equations can be obtained:

$$Re_x^{\frac{1}{2}} C_f = -\frac{1}{(1-\phi)^{2.5}} \hat{F}_2 \Psi(0) = -\frac{1}{(1-\phi)^{2.5}} \hat{F}_2 e_0, \quad Re_x^{\frac{1}{2}} Nu = -\frac{3N+4}{3N} \hat{\Theta}_1 \Psi(0) = -\frac{3N+4}{3N} \hat{\Theta}_1 e_0.$$

The algorithm of the operational matrix-based method to solve two-dimensional incompressible viscous MHD nanofluid flow over a flat sheet is as follows.

Algorithm

Input: $n \in \mathbb{N}, L \in \mathbb{R}^+$.

Output: The barycentric cardinal solutions: $f(\eta) \simeq \hat{F}_0 \Psi(\eta)$ and $\theta(\eta) \simeq \hat{\Theta}_0 \Psi(\eta)$ from (26) and (27), respectively.

Step 1: Set, $a = 0$ and $b = L$.

Step 2: Define $\Delta = \{a = \eta_0 < \eta_1 < \dots < \eta_n = b\}$

where $\eta_j = \frac{L}{2} \left(1 - \cos \left(\frac{j\pi}{n} \right) \right), \quad j = 0, 1, \dots, n.$

Step 3: Construct $\psi_j(\eta), j = 0, 1, \dots, n$ from (9) and define $\Psi(\eta) = [\psi_0(\eta), \psi_1(\eta), \dots, \psi_n(\eta)]^T$.

Step 4: Compute the operational matrix of integration $\mathbf{P} = (p_{ij})$ using (12).

Step 5: Define the unknown vectors $F = [f_0, f_1, \dots, f_n]^T$ and $\Theta = [\theta_0, \theta_1, \dots, \theta_n]^T$.

Step 6: Compute

$$v_{f,k}(\eta) = \sum_{j=1}^k \frac{f^{(s-j)}(a)}{(k-j)!} (\eta - a)^{k-j}, k = 1, 2, 3.$$

Step 7: Compute

$$v_{\theta,k}(\eta) = \sum_{j=1}^k \frac{\theta^{(2-j)}(a)}{(k-j)!} (\eta - a)^{k-j}, k = 1, 2.$$

Step 8: Compute $\Lambda_{f,k}, k = 1, 2, 3$ and $\Lambda_{\theta,k}, k = 1, 2$ from Remark 4.3.

Step 9: Compute $\tilde{F}_{3-k} = (\Lambda_{f,k}^T + F^T \mathbf{P}^k), k = 1, 2, 3$ and $\tilde{\Theta}_{2-k} = (\Lambda_{\theta,k}^T + \Theta^T \mathbf{P}^k), k = 1, 2$.

Step 10: Compute \tilde{B}_1, \tilde{B}_2 and \tilde{B}_3 in (28)-(30) using product operational matrix.

Step 11: Solve the nonlinear algebraic system (31)-(32) and compute the unknown coefficients f_i and θ_i .

6 CONVERGENCE ANALYSIS

In this section the convergence analysis for the applied numerical technique is investigated. As it is clear, the barycentric rational cardinal functions (9) with the weight that introduced by Floater and Hormann, are free of real poles. So, the resulting rational interpolant (8) is infinitely smooth. Cirillo et al. [40] proposed the convergence rate for derivatives of FH-interpolant in the case of well-spaced nodes like Chebyshev-Gauss-Lobatto nodes.

Definition 6.1 Consider $n \in \mathbb{N}$,

$X_n = \{\eta_0, \eta_1, \dots, \eta_n\}$ be a set of interpolation points, $h_{i,j} = |\eta_i - \eta_j|, h_i = h_{i+1,i}, h = \max_{0 \leq i \leq n-1} h_i$.

Then, $X = (X_n)_{n \in \mathbb{N}}$ describes a family of well-spaced nodes if there exist constants $R_1, R_2 \geq 1$ independent of n so that the following conditions hold for every set of nodes X_n :

$$\begin{aligned} \frac{1}{R_1} \leq \frac{h_i}{h_{i-1}} \leq R_1, \quad i = 1, 2, \dots, n-1, \\ \frac{h_i}{h_{i+1,j}} \leq \frac{R_2}{i-j+1}, \quad j = 0, 1, \dots, i, \quad i = 0, 1, \dots, n-1, \\ \frac{h_i}{h_{j,i}} \leq \frac{R_2}{j-i}, \quad j = i+1, i+2, \dots, n, \quad i = 0, 1, \dots, n-1. \end{aligned}$$

Theorem 6.2 [40] Let $n \in \mathbb{N}, d \leq n, 0 \leq k \leq d, f(\eta) \in C^{d+2+k}[a, b]$ and $f_n(\eta)$ be the approximation solution obtained by FH-interpolant (8). Then, for any set of well-spaced interpolation nodes,

$$\|f^{(k)}(\eta) - f_n^{(k)}(\eta)\|_{\infty} \leq Ch^{d+1-k}, \quad (33)$$

where C is a constant dependent on k, d , the derivative of $f(\eta)$ and the constants R_1 and R_2 that defined in Definition 6.1.

Suppose that $f \in C^{d+5}[0, L], \theta \in C^{d+4}[0, L]$ and $f_n(\eta)$ and $\theta_n(\eta)$ are the obtained approximation solutions of $f(\eta)$ and $\theta(\eta)$ respectively by using the FH-interpolant (8). The residual functions of the differential equations (1) and (2) will be represented as

$$\begin{aligned} \text{RES}_f(\eta) &= (f_n'''(\eta) - f'''(\eta)) + (1 - \phi)^{2.5} L_1 f(\eta) (f_n''(\eta) - f''(\eta)) \\ &\quad - (1 - \phi)^{2.5} (L_1 (f_n'(\eta) + f'(\eta)) + Mn) (f_n'(\eta) - f'(\eta)) \\ &\quad + (1 - \phi)^{2.5} L_1 f_n''(\eta) (f_n(\eta) - f(\eta)) + (1 - \phi)^{2.5} \lambda L_2 (\theta_n(\eta) - \theta(\eta)), \end{aligned}$$

$$\begin{aligned} \text{RES}_\theta(\eta) &= (\theta_n''(\eta) - \theta''(\eta)) + \frac{3N}{3N+4} \frac{k_f}{k_{nf}} PrL_2 f(\eta) (\theta_n'(\eta) - \theta'(\eta)) \\ &\quad + \frac{3N}{3N+4} \frac{k_f}{k_{nf}} PrL_2 \theta_n'(\eta) (f_n(\eta) - f(\eta)), \end{aligned}$$

where $L_1 = 1 - \phi + \frac{\rho_s}{\rho_f} \phi$ and $L_2 = 1 - \phi + \frac{(\rho C_p)_s}{(\rho C_p)_f} \phi$.

Due to Theorem 6.2 there is constants $C_j, j = 1, 2, \dots, 6$ such that

$$\begin{aligned} \|\text{RES}_f\|_{\infty} \leq &\|f_n''' - f'''\|_{\infty} + C_1 \|f_n'' - f''\|_{\infty} + C_2 \|f_n' - f'\|_{\infty} \\ &+ C_3 \|f_n - f\|_{\infty} + C_4 \|\theta_n - \theta\|_{\infty} = O(h^{d-2}), \end{aligned}$$

$$\|\text{RES}_\theta\|_{\infty} \leq \|\theta_n'' - \theta''\|_{\infty} + C_5 \|f_n - f\|_{\infty} + C_6 \|\theta_n' - \theta'\|_{\infty} = O(h^{d-1}),$$

where

$$\begin{aligned} |(1 - \phi)^{2.5} L_1| \|f(\eta)\|_{\infty} &\leq C_1, \\ |(1 - \phi)^{2.5}| \|L_1 (f_n'(\eta) + f'(\eta)) + Mn\|_{\infty} &\leq C_2, \\ |(1 - \phi)^{2.5} L_1| \|f_n''(\eta)\|_{\infty} &\leq C_3, \\ |(1 - \phi)^{2.5} \lambda L_2| &\leq C_4, \end{aligned}$$

$$\begin{aligned} \left| \frac{3N}{3N+4} \frac{k_f}{k_{nf}} PrL_2 \right| \|f(\eta)\|_{\infty} &\leq C_5, \\ \left| \frac{3N}{3N+4} \frac{k_f}{k_{nf}} PrL_2 \right| \|\theta_n'(\eta)\|_{\infty} &\leq C_6. \end{aligned}$$

Thus, we have

$$\|\text{RES}_f\|_{\infty} \rightarrow 0, \quad \text{and} \quad \|\text{RES}_\theta\|_{\infty} \rightarrow 0, \quad \text{as } h \rightarrow 0.$$

7 NUMERICAL RESULTS AND DISCUSSION

In this section, the influences of different embedding parameters on the velocity profile f , temperature distribution θ , skin friction coefficient C_f and Nusselt number Nu are investigated. Also, to verify efficiency and high accuracy of the barycentric cardinal functions method, the results of the proposed method (PM) on the interval $[0, L]$ are compared with the numerical results based on Maple's dsolve (type=numeric) command. Here, the shifted Chebyshev-Gauss-Lobatto nodes was used as follow:

$$\eta_j = \frac{L}{2} \left(1 - \cos\left(\frac{j\pi}{n}\right) \right), \quad j = 0, 1, \dots, n,$$

Table 1: Thermo-physical properties of pure water and nanoparticle [50]

	$\rho(Kg/m^3)$	$C_p(J/Kg K)$	$k(W/m K)$	$\beta \times 10^5(K^{-1})$
Copper (Cu)	8933	385	401	1.67
Copper oxide (CuO)	6320	531.8	76.5	1.80
Pure water	997.1	4179	0.613	21

Fig. 2 depicts the effect of different values of Mn on the velocity profile $f(\eta)$ and temperature distribution $\theta(\eta)$ for Cu-water and CuO-water. The increase of the magnetic parameter leads to a decrease in the velocity profile and an increase in the temperature distribution at all points for both Cu and CuO nanofluids. As a result of the increase

to construct the barycentric rational cardinal functions (9) and compute the relative error percentage (RE(%)) from the following formula:

$$RE(\%) = \frac{|PM \text{ results} - \text{Numerical results}|}{|\text{Numerical results}|} \times 100.$$

The thermo-physical properties of the nanofluids and the base fluid are given in Table 1. Copper (Cu) and copper oxide (CuO) act as nanoparticles and water is the base fluid.

in temperature, the thermal boundary layers become thick. According to Fig. 2, the velocity profile for CuO nanoparticle is higher than of Cu nanoparticle and the difference in temperature distribution between Cu and CuO nanoparticles is negligible.

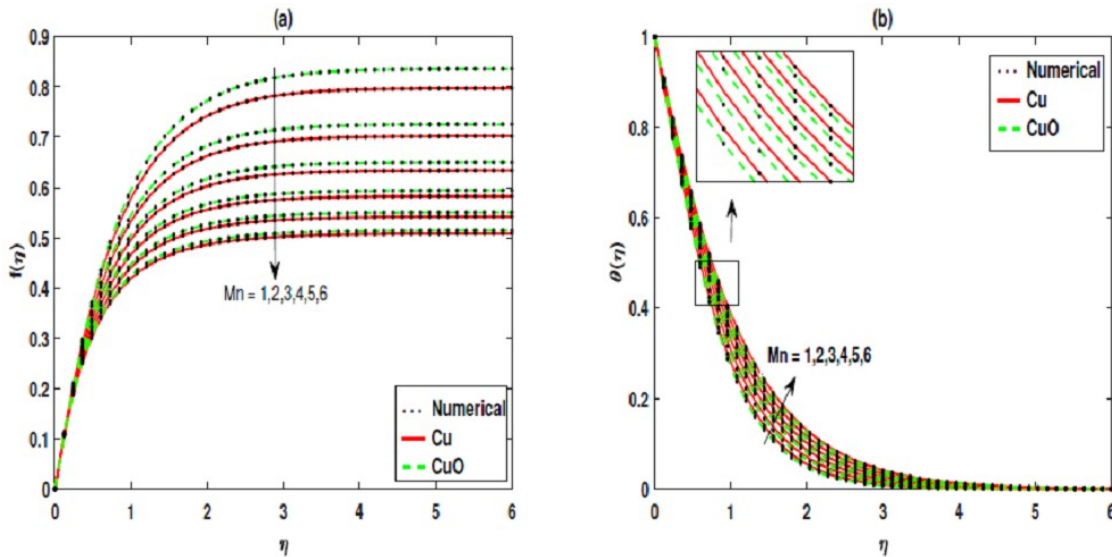


Fig. 2: The velocity profile f (a) and temperature distribution θ (b) for different values of Mn when $Pr = 6.2, N = 2, \lambda = 1, \phi = 0.12, n = 20, d = 18$ and $L = 6$.

Fig. 3 displays the effect of different values of λ on $f(\eta)$ and $\theta(\eta)$. For both Cu and CuO nanoparticles, increasing the buoyancy parameter increases the velocity profile and reduces the temperature distribution. Therefore, by

increasing, the boundary layer becomes thicker and the thermal boundary layer becomes thinner. As it is clear, the velocity profile for Cu-water is lower than CuO-water and the difference in temperature distribution for Cu and CuO nanoparticles is inconsiderable.

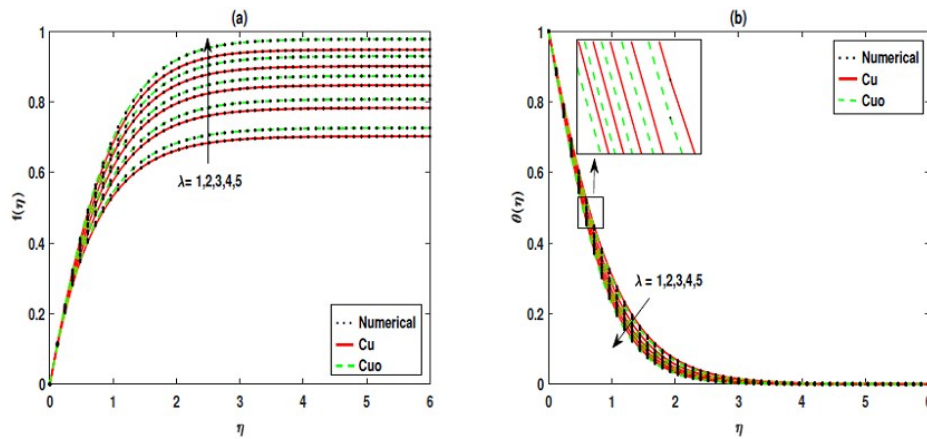


Fig. 3: The velocity profile f (a) and temperature distribution θ (b) for different values of λ when $Pr = 6.2, N = 2, Mn = 2, \phi = 0.12, n = 20, d = 18$ and $L = 6$.

The effect of different values of ϕ on $f(\eta)$ and $\theta(\eta)$ for Cu and CuO nanoparticles is illustrated in Figs. 4-5. Fig. 4 reveals that, by applying higher magnetic parameter and increasing η , the velocity profile and temperature distribution increase for both Cu and CuO nanoparticles.

According to Fig. 5, it is clear that with increasing η along with the small amount of the magnetic parameter, the velocity decreases and temperature distribution increases. Therefore, increasing η in the presence of magnetic parameter causes the thermal boundary layer to thicken.

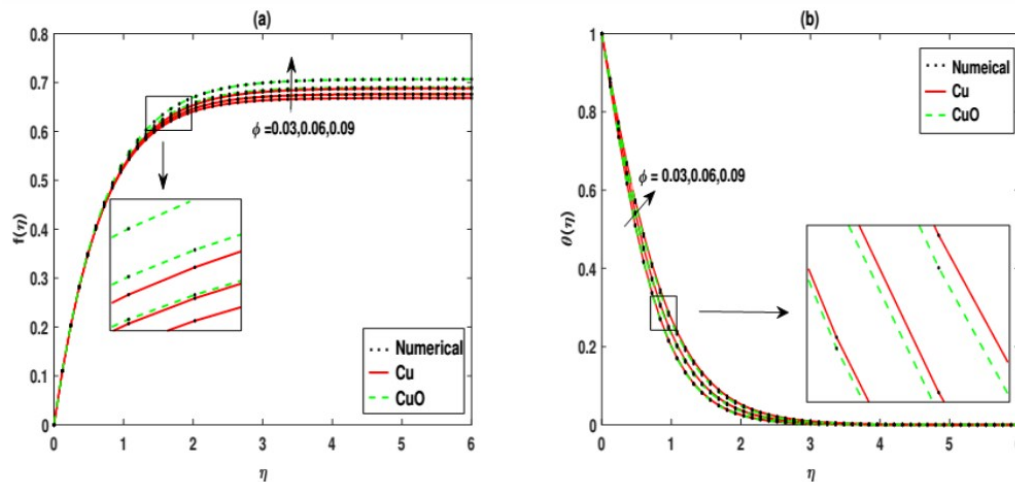


Fig.4: The velocity profile f (a) and temperature distribution θ (b) for different values of ϕ when $Pr = 6.2, N = 2, Mn = 2, \lambda = 1, n = 20, d = 18$ and $L = 6$.

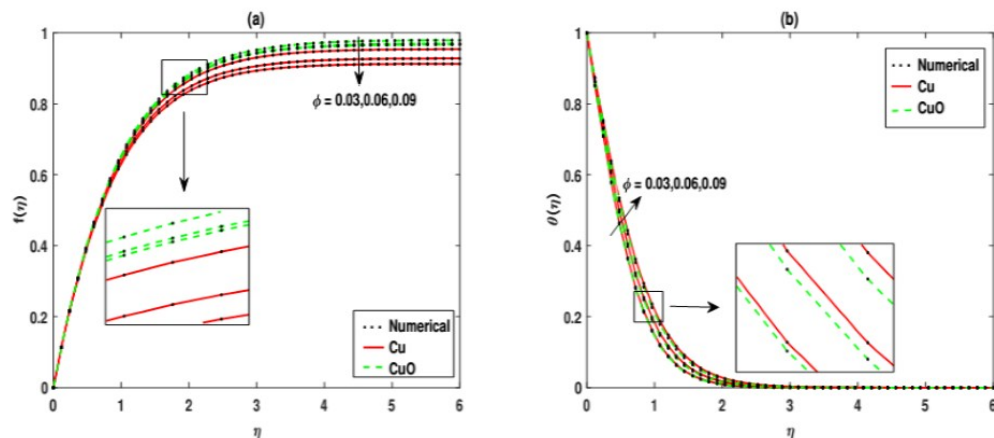


Fig. 5: The velocity profile f (a) and temperature distribution θ (b) for different values of ϕ when $Pr = 6.2, N = 2, Mn = 0.2, \lambda = 1, n = 20, d = 18$ and $L = 6$.

The effect of different values of N on the temperature distribution is represented in Fig. 6. For both Cu and CuO

nanoparticles, increasing the radiation parameter reduces $\theta(\eta)$ and thins the thermal boundary layer.

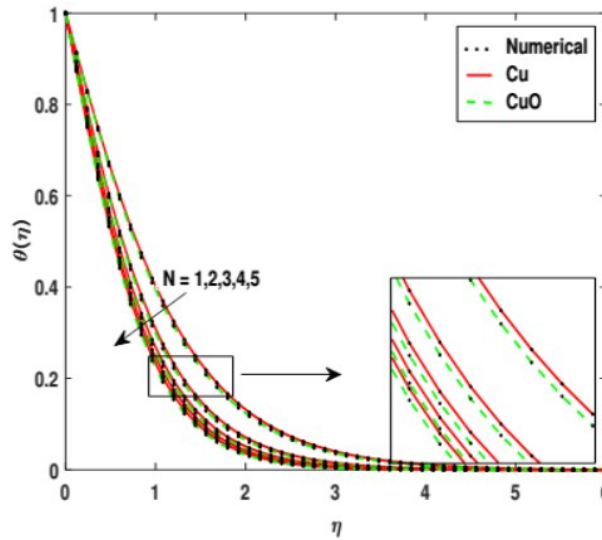


Fig. 6: The temperature distribution θ for different values of N when $Pr = 6.2$, $\phi = 0.12$, $Mn = 2$, $\lambda = 1$, $n = 20$, $d = 18$ and $L = 6$.

The effect of parameters Mn and ϕ on the Nusselt number and skin friction coefficient is shown in Fig. 7. By increasing, the skin friction coefficient increases and the

Nusselt number decreases. Also, increasing with a constant magnetic parameter leads to a decrease of the Nusselt number and an increase of the skin friction coefficient.

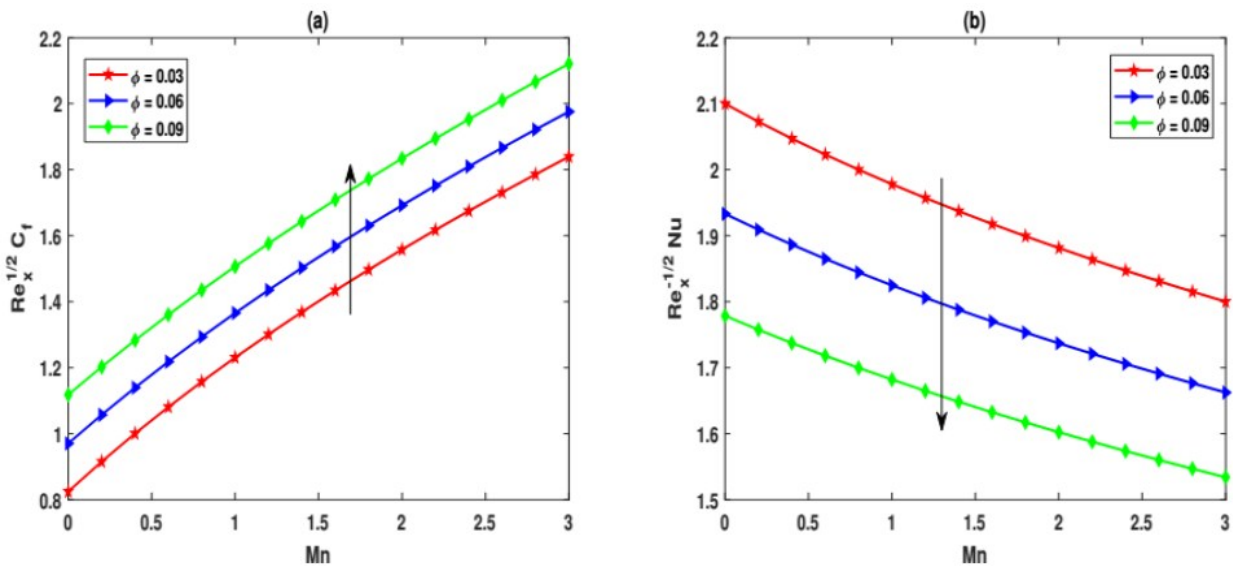


Fig. 7: The skin friction coefficient (a) and Nusselt number (b) for different values of ϕ and Mn of Cu-water when $Pr = 6.2$, $N = 2$, $\lambda = 1$, $n = 36$, $d = 34$ and $L = 6$.

Tables 2- 4 give a comparison between the proposed method and the numerical method for the skin friction coefficient and the reduced Nusselt number. These tables reveal that the results of the proposed method are in good

agreement with the numerical results based on Maple's dsolve and Runge-Kutta method results that described in [50].

Table 2: Comparison between the proposed method and numerical results for $-f''(0)$ with $n = 40, d = 38, Pr = 6.2$ and $L = 13.5$ for Cu-Water.

	Runge-Kutta [50]	PM	Maple's dsolve	RE(%)
$\lambda = 1, N = 2, \phi = 0.12$				
$Mn = 1$	1.20278694	1.2027869326	1.2027869328	$9.86e - 08$
$Mn = 2$	1.44214325	1.4421432504	1.4421432503	$6.93e - 09$
$Mn = 3$	1.65402315	1.6540231544	1.6540231542	$1.20e - 08$
$Mn = 2, \lambda = 1, N = 2$				
$\phi = 0.00$	-	1.4312534805	1.4312534749	$3.85e - 07$
$\phi = 0.02$	-	1.4404884133	1.4404884105	$1.92e - 07$
$\phi = 0.03$	-	1.4439037405	1.4439037385	$1.35e - 07$
$\phi = 0.04$	-	1.4465467242	1.4465467228	$9.62e - 08$
$\phi = 0.05$	-	1.4484377888	1.4484377879	$6.83e - 08$
$\phi = 0.10$	1.44726274	1.4472627358	1.4472627356	$1.38e - 08$
$Mn = 2, N = 2, \phi = 0.03$				
$\lambda = 0$	-	1.7324259629	1.7324259629	$1.68e - 17$
$\lambda = 1$	-	1.4439037405	1.4439037385	$1.35e - 07$
$\lambda = 2$	-	1.1729579110	1.1729579109	$2.01e - 09$
$Mn = 2, \lambda = 1, \phi = 0.03$				
$N = 1$	-	1.4118494552	1.4118494550	$8.05e - 09$
$N = 2$	-	1.4439037405	1.4439037385	$1.35e - 07$
$N = 3$	-	1.4574373005	1.4574372944	$4.14e - 07$

Table 3: Comparison between the proposed method and numerical results for $-f'''(0)$ with $n = 40, d = 38, Pr = 6.2$ and $L = 13.5$ for CuO-Water.

	PM	Maple's dsolve	RE(%)
$\lambda = 1, N = 2, \phi = 0.03$			
$Mn = 1$	1.1154342246	1.1154342262	$1.43e - 07$
$Mn = 2$	1.4232863684	1.4232863666	$1.30e - 07$
$Mn = 3$	1.6867767932	1.6867767913	$1.16e - 07$
$Mn = 2, \lambda = 1, N = 2$			
$\phi = 0.00$	1.4312534805	1.4312534749	$3.85e - 07$
$\phi = 0.02$	1.4263970974	1.4263970947	$1.88e - 07$
$\phi = 0.03$	1.4232863684	1.4232863666	$1.30e - 07$
$\phi = 0.04$	1.4197298752	1.4197298739	$8.93e - 08$
$\phi = 0.05$	1.4157343788	1.4157343779	$6.08e - 08$
$\phi = 0.10$	1.3893986127	1.3893986126	$7.91e - 09$
$Mn = 2, N = 2, \phi = 0.03$			
$\lambda = 0$	1.7112703095	1.7112703095	$1.20e - 17$
$\lambda = 1$	1.4232863684	1.4232863666	$1.30e - 07$
$\lambda = 2$	1.1526391378	1.1526391383	$4.47e - 08$
$Mn = 2, \lambda = 1, \phi = 0.03$			
$N = 1$	1.3911677398	1.3911677398	$6.13e - 09$
$N = 2$	1.4232863684	1.4232863666	$1.30e - 07$
$N = 3$	1.4368354630	1.4368354571	$4.13e - 07$

Table 4: Comparison between the proposed method and numerical results for $-\theta'(0)$ with $n = 40, d = 38, Pr = 6.2$ and $L = 13.5$.

	PM	Cu-Water Maple's dsolve	RE(%)	PM	CuO-Water Maple's dsolve	RE(%)
$\lambda = 1, N = 2, \phi = 0.03$						
$Mn = 1$	1.1868917613	1.1868917541	6.10 e-07	1.1931817185	1.1931817115	5.90e-07
$Mn = 2$	1.1288138212	1.1288138160	4.55 e-07	1.1340180894	1.1340180839	4.88e-07
$Mn = 3$	1.0800143822	1.0800143819	3.10 e-08	1.0845041457	1.0845041450	6.15e-08
$Mn = 2, \lambda = 1, N = 2$						
$\phi = 0.00$	1.2220889094	1.2220888952	1.16 e-06	1.2220889094	1.2220888952	1.16e-06
$\phi = 0.02$	1.1591144941	1.1591144868	6.26 e-07	1.1626848028	1.1626847951	6.57e-07
$\phi = 0.03$	1.1288138212	1.1288138160	4.55 e-07	1.1340180894	1.1340180839	4.88e-07
$\phi = 0.04$	1.0992530377	1.0992530340	3.29 e-07	1.1059970445	1.1059970405	3.61e-07
$\phi = 0.05$	1.0703962984	1.0703962958	2.37 e-07	1.0785903882	1.0785903854	2.65e-07
$\phi = 0.10$	0.9355357619	0.9355357615	4.36 e-08	0.9497781861	0.9497781855	5.34e-08
$Mn = 2, N = 2, \phi = 0.03$						
$\lambda = 0$	1.0711438841	1.0711438846	5.44 e-08	1.0768256498	1.0768256500	1.89e-08
$\lambda = 1$	1.1288138212	1.1288138160	4.55 e-07	1.1340180894	1.1340180839	4.88e-07
$\lambda = 2$	1.1739889099	1.1739888993	8.99 e-07	1.1789900044	1.1789899936	9.15e-07
$Mn = 2, \lambda = 1, \phi = 0.03$						
$N = 1$	0.9186658181	0.9186658178	3.21 e-08	0.9233521556	0.9233521553	3.42e-08
$N = 2$	1.1288138212	1.1288138160	4.55 e-07	1.1340180894	1.1340180839	4.88e-07
$N = 3$	1.2311303826	1.2311303680	1.18 e-06	1.2365378935	1.2365378777	1.27e-06

Also, from Table 5, it is clear that the results of the proposed method in comparison with the numerical results which represented in [53] and [54], are in good agreement with the analytical results that reported in [13].

Table 5: Comparison results for $-\theta'(0)$ with $Mn = \lambda = \phi = 0, n = 46$ and $d = 44$.

Pr	L	PM	Hamad [13]	Wang [53]	Gorla et. al [54]
7.00	13.00	1.8954030	1.89540	1.8954	1.8905
20.0	10.00	3.3539041	3.35390	3.3539	3.3539
70.0	10.92	6.4621975	6.46220	6.4622	6.4622

8 CONCLUSION

In this research, the steady two-dimensional viscous incompressible MHD nanofluid along a semi-infinite vertical stretching sheet accompanied by thermal radiation and buoyancy parameter has been studied. The barycentric rational cardinal functions with associated operational matrices of integration and product were employed to approximate the numerical solutions of the governing nonlinear differential equations. The advantage of the proposed method is that, without using any collocation points, the system of differential equations is converted to the system of algebraic equations. An appropriate agreement between the results of the proposed method and the numerical method by using Maple's dsolve, the analytical results in [13] and the numerical results in [50], [53] and [54] confirms the accuracy and efficiency of the proposed scheme. The summary of the obtained results from this research is as follows:

- Increasing Mn decreases the velocity profile thickness and increases the temperature distribution. Therefore, by increasing magnetic

parameter, the thermal boundary layer becomes thicker.

- An enhancement in λ increases the velocity profile and vice versa decreases the temperature distribution. So, the velocity boundary layer becomes thick and thermal boundary layer becomes thin.
- By increasing ϕ , the velocity profile increases if the magnetic parameter is high and vice versa the velocity profile decreases if the magnetic parameter is small. In both cases, the increase of makes the temperature to enhance and results in thickening of the thermal layer.
- Increasing the radiation parameter results in a decrease in the temperature.
- The velocity profile with copper oxide nanoparticles is higher than copper nanoparticles, while changes in temperature distribution with copper and copper oxide nanoparticles are negligible.

Nomenclature

u	Velocity component in the x direction
v	Velocity component in the y direction
T	Temperature
T_w	Temperature of sheet
T_∞	The ambient temperature
f	Dimensionless velocity
Re_x	Local Reynolds number
Pr	Prandtl number
Nu	Nusselt number
N	Radiation parameter
C_p	Specific heat
C_f	Skin friction coefficient
k	Thermal conductivity
k^*	Mean absorption coefficient
B_0	Magnetic field
Greek symbols	
θ	Cylindrical coordinate
σ	Stefan-Boltzmann constant,
η	Dimensionless angle
ρ	Density
μ	Dynamic viscosity
ν	Kinematic viscosity
ϕ	Solid volume fraction
Subscripts	
nf	Nanofluid
f	Base fluid
s	Nano-solid-particle

References

- [1] B. C. Sakiadis, Boundary-layer behavior on continuous solid surface: I. boundary-layer equations for two-dimensional and axisymmetric flow, *AICHE Journal*, 7 (1961) 26-28.
- [2] B. C. Sakiadis, Boundary layer behavior on continuous solid surfaces: II. boundary layer on a continuous flat surface, *AICHE Journal*, 7 (1961) 221-225.
- [3] L. J. Crane, Flow past a stretching plate, *Applied Mathematics and Physics*, 21 (1970) 645-647.
- [4] B. S. Dandapat, A. S. Gupta, Flow and heat transfer in a viscoelastic fluid over a stretching sheet, *International Journal of Non-Linear Mechanics*, 24 (1989) 215-219.
- [5] B. Bidin, Numerical solution of the boundary layer flow over an exponentially stretching sheet with thermal radiation, *European Journal of Scientific Research*, 33 (2009) 710-717.
- [6] T. Hayat, Q. Hussain, T. Javed, The modified decomposition method and Pade approximants for the MHD flow over a non-linear stretching sheet, *Nonlinear Analysis: Real World Applications*, 10 (2009) 966-973.
- [7] N. F. M. Noor, I. Hashim, MHD viscous flow over a linearly stretching sheet embedded in a non-Darcian porous medium, *Journal of Porous Media*, 13 (2010) 349-355.
- [8] M. M. Rashidi, E. Erfani, The modified differential transform method for investigating nano boundary-layers over stretching surfaces, *International Journal of Numerical Methods for Heat & Fluid Flow*, 21 (2011) 864-883.
- [9] N. F. M. Noor, I. Hashim, ADM solution for MHD boundary layer flow over a nonlinearly stretching sheet in the presence of viscous dissipation, *AIP Conference Proceedings* 1750, 030019 (2016).
- [10] M. Heydari, G. B. Loghmani, A. A. Dehghan, Numerical study of generalized three-dimensional MHD flow over a porous stretching sheet, *Journal of Applied Fluid Mechanics*, 7 (2014) 473-483.
- [11] E. Hosseini, G. B. Loghmani, M. Heydari, M. M. Rashidi, Numerical investigation of velocity slip and temperature jump effects on unsteady flow over a stretching permeable surface, *The European Physical Journal Plus*, 132 (2017) 96.
- [12] W. A. Khan, I. Pop, Boundary-layer flow of a nanofluid past a stretching sheet, *International Journal of Heat and Mass Transfer*, 53 (2010) 2477-2483.
- [13] M. A. A. Hamad, Analytical solution of natural convection flow of a nanofluid over a linearly stretching sheet in the presence of magnetic field, *International Communications in Heat and Mass Transfer*, 38 (2011) 487-492.
- [14] M. M. Rashidi, A. K. Abdul Hakeem, N. Vishnu Ganesh, B. Ganga, M. Sheikholeslami, E. Momoniat, Analytical and numerical studies on heat transfer of a nanofluid over a stretching/shrinking sheet with second-order slip flow model, *International Journal of Mechanical and Materials Engineering*, 11 (2016) 1-14.
- [15] P. Rana, R. Bhargava, Flow and heat transfer of a nanofluid over a nonlinearly stretching sheet: A numerical study, *Communications in Nonlinear Science and Numerical Simulation*, 17 (2012) 212-226.
- [16] T. Hayat, M. Imtiaz, A. Alsaedi, R. Mansoor, MHD flow of nanofluids over an exponentially stretching sheet in a porous medium with convective boundary conditions, *Chinese Physics B*, 23 (2014) 054701.
- [17] C. S. Reddy, K. Naikotib, M. M. Rashidi, MHD flow and heat transfer characteristics of Williamson nanofluid over a stretching sheet with variable thickness and variable thermal conductivity, *Transactions of A. Razmadze Mathematical Institute*, 171 (2017) 195-211.
- [18] T. Hayat, M. Rashid, A. Alsaedi, B. Ahmad, Flow of nanofluid by nonlinear stretching velocity, *Results in Physics*, 8 (2018) 1104-1109.
- [19] M. Lakestani, M. Dehghan, Numerical solution of Riccati equation using the cubic Bspline scaling functions and Chebyshev cardinal functions, *Computer Physics Communications*, 181(5) (2010) 957-966.
- [20] M. Heydari, G. B. Loghmani, S. M. Hosseini, Operational matrices of Chebyshev cardinal functions and their application for solving delay differential equations arising in electrodynamics with error estimation, *Applied Mathematical Modelling*, 37 (2013) 7789-7809.
- [21] Z. Avazzadeh, M. Heydari, Chebyshev cardinal functions for solving age-structured population models, *International Journal of Applied and Computational Mathematics*, 3 (2017) 2139-2149.
- [22] M. Heydari, G. B. Loghmani, S. M. Hosseini, S. M. Karbassi, Application of hybrid functions for solving diffing-harmonic oscillator, *Journal of Difference Equations*, Hindawi, 2014, Article ID 210754, 1-9.
- [24] M. Heydari, G. B. Loghmani, S.M. Hosseini, S.M. Karbassi, Direct method to solve differential-algebraic equations by using the operational matrices of Chebyshev cardinal functions, *Journal of Mathematical Extension*, 7 (2013) 25-47.
- [24] H. Heydari, Z. Avazzadeh, G. B. Loghmani, Chebyshev cardinal functions for solving volterra-fredholm integrodifferential equations using operational matrices,

- Iranian Journal of Science and Technology, Transaction A: Science, 36 (2012) 13-24.
- [25] Z. Nikooeinejad, A. Delavarkhalafi, M. Heydari, A numerical solution of open-loop Nash equilibrium in nonlinear differential games based on Chebyshev pseudospectral method, *Journal of Computational and Applied Mathematics*, 300 (2016) 369-384.
- [26] Z. Nikooeinejad, A. Delavarkhalafi, M. Heydari, Application of shifted Jacobi pseudospectral method for solving (in)finite-horizon minmax optimal control problems with uncertainty, *International Journal of Control*, 91 (2017) 725-739.
- [27] Z. Nikooeinejad, M. Heydari, Nash equilibrium approximation of some class of stochastic differential games: A combined Chebyshev spectral collocation method with policy iteration, *Journal of Computational and Applied Mathematics*, 362 (2019) 41-54.
- [28] Z. Avazzadeh, M. Heydari, Chebyshev polynomials for solving two dimensional linear and nonlinear integral equations of the second kind, *Computational and Applied Mathematics*, 31 (2012) 127-142.
- [29] M. Heydari, G. B. Loghmani, S. M. Hosseini, A. Yildirim, A novel hybrid spectral-variational iteration method (H-S-VIM) for solving nonlinear equations arising in heat transfer, *Iranian Journal of Science and Technology, Transactions A: Science* 37 (2013) 501- 512.
- [30] M. Heydari, G. B. Loghmani, M. M. Rashidi, S. M. Hosseini, A numerical study for off-centered stagnation flow towards a rotating disc, *Journal of Propulsion and Power*, 4 (2015) 169-178.
- [31] E. Hosseini, G. B. Loghmani, M. Heydari, A. M. Wazwaz, A numerical study of electrohydrodynamic flow analysis in a circular cylindrical conduit using orthonormal Bernstein polynomials, *Computational Methods for Differential Equations*, 5 (2017) 280-300.
- [32] M. Heydari, G. B. Loghmani, S. M. Hosseini, Exponential Bernstein functions: an effective tool for the solution of heat transfer of a micropolar fluid through a porous medium with radiation, *Computational and Applied Mathematics*, 36 (2017) 647-675.
- [33] E. Hosseini, G. B. Loghmani, M. Heydari, M. M. Rashidi, Investigation of magneto-hemodynamic flow in a semi-porous channel using orthonormal Bernstein polynomials, *The European Physical Journal Plus*, 132 (2017) 326.
- [34] Z. Avazzadeh, M. Heydari, G. B. Loghmani, A Comparison between solving two dimensional integral equations by the traditional collocation method and radial basis functions, *Applied Mathematical Sciences*, 5 (2011) 1145-1152.
- [35] M. Heydari, S. M. Hosseini, G. B. Loghmani, Numerical solution of singular IVPs of Lane-Emden type using integral operator and radial basis functions, *International Journal of Industrial Mathematics*, 4 (2012) 135-146.
- [36] Z. Avazzadeh, M. Heydari, W. Chen, G. B. Loghmani, Smooth solution of partial integro-differential equations using radial basis functions, *Journal of Applied Analysis and Computation*, 4 (2014) 115-127.
- [37] C. Schneider, W. Werner, Some new aspects of rational interpolation, *Mathematics of computation*, 47 (1986) 285-299.
- [38] J. P. Berrut, Rational function for guaranteed and experimentally well-conditioned global interpolation, *Computers & Mathematics with Applications*, 15 (1988) 1-16.
- [39] M. S. Floater, K. Hormann, Barycentric rational interpolation with no poles and high rates of approximation, *Numerische Mathematik*, 107 (2007) 315-331.
- [40] E. Cirillo, K. Hormann, J. Sidon, Convergence rates of derivatives of Floater-Hormann interpolants for well-spaced nodes, *Applied Numerical Mathematics*, 116 (2017) 108-118.
- [41] J. P. Berrut, H. D. Mittermann, The linear rational pseudospectral method with iteratively optimized poles for two-point boundary value problems, *SIAM Journal Scientific Computing*, 23 (2001) 961-975.
- [42] W. Ma, B. Zhang, H. Ma, A meshless collocation approach with barycentric rational interpolation for two-dimensional hyperbolic telegraph equation, *Applied Mathematics and Computation*, 279 (2016) 236-248.
- [43] J. P. Berrut, S. A. Hosseini, G. Klein, The linear barycentric rational quadrature method for Volterra integral equations, *SIAM Journal on Scientific Computing*, 36 (2014) A105-A123.
- [44] H. Liu, J. Huang, Y. Pan, J. Zhang, Barycentric interpolation collocation methods for solving linear and nonlinear high-dimensional Fredholm integral equations, *Computational and Applied Mathematics* 327 (2018) 141-154.
- [45] A. Abdi, S. A. Hosseini, The barycentric rational difference-quadrature scheme for systems of Volterra integro-differential equations, *SIAM Journal on Scientific Computing*. 40 (2018) A1936-A1960.
- [46] A. Rezaei, F. Baharifard, K. Parand, Quasilinearization Barycentric approach for numerical investigation of the boundary value fin problem, *International Journal of Computer, Electrical, Automation, Control and Information Engineering*, 5 (2011) 194-201.
- [47] S. Torkaman, G. B. Loghmani, M. Heydari, M. M. Rashidi, Novel numerical solutions of nonlinear heat transfer problems using the linear barycentric rational interpolation, *Heat Transfer-Asian Res*, 48 (2019) 1318-1344.
- [48] J. P. Boyd, *Chebyshev and Fourier Spectral Methods*, Dover Publications, Inc., (2000).
- [49] C. Canuto, M. Y. Hussaini, Q. Alfio, and A. Z. Thomas, *Spectral methods in fluid dynamics*, Springer series in computational physics, Springer-Verlag, Berlin, 1991.
- [50] M. M. Rashidi, N. Vishnu Ganesh, A. K. Abdul Hakeem, B. Ganga, Buoyancy effect on MHD flow of nanofluid over a stretching sheet in the presence of thermal radiation, *Journal of Molecular Liquids*, 198 (2014) 234-238.
- [51] A. K. Abdul Hakeem, N. Vishnu Ganesh, B. Ganga, Effect of heat radiation in a Walter's liquid B fluid over a stretching sheet with non-uniform heat source/sink and elastic deformation, *Journal of King Saud University- Engineering Sciences*, 26 (2014) 168-175.
- [52] N. Vishnu Ganesh, B. Ganga, A. K. Abdul Hakeem, Lie symmetry group analysis of magnetic field effects on free convective flow of a nanofluid over a semi-infinite stretching sheet, *Journal of the Egyptian Mathematical Society*, 22 (2014) 304-310.
- [53] C. Y. Wang, Free convection on a vertical stretching surface, *Journal of Applied Mathematics and Mechanics*, 69 (1989) 418-420.
- [54] R. S. R. Gorla, I. Sidawi, Free convection on a vertical stretching surface with suction and blowing, *Applied Scientific Research*, 52 (1994) 247-257.



This document was created with the Win2PDF "print to PDF" printer available at <http://www.win2pdf.com>

This version of Win2PDF 10 is for evaluation and non-commercial use only.

This page will not be added after purchasing Win2PDF.

<http://www.win2pdf.com/purchase/>